Ocean Systems Engineering, *Vol. 13, No. 4 (2023) 401-421*
https://doi.org/10.12989/ose.2023.13.4.401

Fully coupled multi-hull/mooring/riser/hawser time domain simulation of TLP-TAD system with MR damper

Muhammad Zaid Zainuddin*[1], Moo-Hyun Kim[1], Chungkuk Jin[1] and Shankar Bhat[2]

[1]Department of Ocean Engineering, Texas A&M University,
727 Ross Street, College Station, TX 77843, United States of America
[2]Offshore Structures, Hull, Riser & Mooring (OHR&M) Deepwater Projects Shell Petroleum Development Company, 21/22 Marina, Lagos, Nigeria

(Received November 19 2023, Revised December 15, 2023, Accepted December 17, 2023)

Abstract. Reducing hawser line tensions and dynamic responses to a certain level is of paramount importance as the hawser lines provide important structural linkage between 2 body TLP-TAD system. The objective of this paper is to demonstrate how MR Damper can be utilized to achieve this. Hydrodynamic coefficients and wave forces for two bodies including second-order effects are obtained by 3D diffraction/radiation panel program by potential theory. Then, multi-hull-riser-mooring-hawser fully-coupled time-domain dynamic simulation program is applied to solve the complex two-body system's dynamics with the Magneto-Rheological (MR) Damper modeled on one end of hawser. Since the damping level of MR Damper can be changed by inputting different electric currents, various simulations are conducted for various electric currents. The results show the reductions in maximum hawser tensions with MR Damper even for passive control cases. The results also show that the hawser tensions and MR Damper strokes are affected not only by input electric currents but also by initial mooring design. Further optimization of hawser design with MR Damper can be done by active MR-Damper control with changing electric currents, which is the subject of the next study.

Keywords: hawsers; hawser tension; magnetorheological damper; MR damper; multi-body system; station keeping

1. Introduction

The use of Tender Assist Drilling (TAD) with dry-tree platforms has been considered a competitive option for field developments in a benign environment. This option offers cost savings through a reduction in dry-tree platform payload. While their use in shallow water alongside jacket platform is ubiquitous, there have been quite a few deepwater projects that utilized a semi-submersible TAD vessel alongside moored/tethered floating platforms (Ravikiran *et al*. 2018).

The use of moored TAD vessel next to a large moored/tethered floating platform brings a unique set of challenges, primarily in the coupling effect of the two platforms and the connection lines between them i.e., soft nylon hawser lines. One particular challenge is related to the relative surge

*Corresponding author, Dr., E-mail: zaidzainuddin@tamu.edu

http://www.techno-press.org/?journal=ose&subpage=7 ISSN: 2093-6702 (Print), 2093-677X (Online)

motion with free-one-end connection bridge and potentially considerable hawser tension, as discussed in this paper.

The hawser lines play an important role in the dynamic positioning of the TAD and moored/tethered platform by providing structural linkage that allows one vessel to pull the other vessel to the desired location. Thus, maintaining the hawser line structural integrity is important. One of the possible structural failures of the hawser line is snapping, which can occur when the hawser's static tension is too low followed by sudden increase in relative surge displacements. In this regard, developing a method to predict the nonlinear dynamic tensions on hawsers in time domain is essential to maintain overall structural integrity, which is our motivation for the present study.

Conventional mechanical viscous damper is widely used to suppress motion by dissipating the dynamic energy. Damper application in tensioned line primarily serves for suppressing axial vibration. Shan *et al.* (2019) studied the relationship between bridge suspender tension and vibration with damper Shan *et al.* (2019). Further studies on damper in tensioned line were also made for the sake of understanding the effect of dampers on the vibration mode. Krenk studied vibrations of taut cable with external damper (Krenk 2000). In these studies, the damping ratio, determined from the complex eigenvalues, is shown to play a role in the classical beam modal analysis. Main and Jones formulated and studied the effect of intermediate damper on the vibration of tensioned beam (Main and Jones 2007),

MR Damper is a semi-active structural damper filled with magneto-rheological fluid (MR fluid), a type of fluid that exhibits viscoelastic behavior when subject to magnetic field (Wang and Liao 2011). The magnetic field is generated when applying electric current to the MR Damper. The viscoelasticity of the MR fluid then determines the damping coefficient of the MR Damper. This means that the MR damping coefficient can be adjusted by adjusting the electric current. This can result in a type of smart damper. Fig. 1 shows a typical schematic of MR Damper.

MR Damper's ability to adjust its damping level provides an opportunity for tension regulation. Currently, the use of MR Damper can be found primarily in vibration suppression in buildings, cars, and offshore structures (Yang *et al*. 2013). Bitaraf *et al*. (2009) demonstrated MR Damper's ability to suppress seismic vibrations of buildings (Bitaraf *et al*. 2009). JZ20-2NW in Bohai Gulf, China is the first offshore structure incorporating MR Dampers, coupled with rubber isolators between main

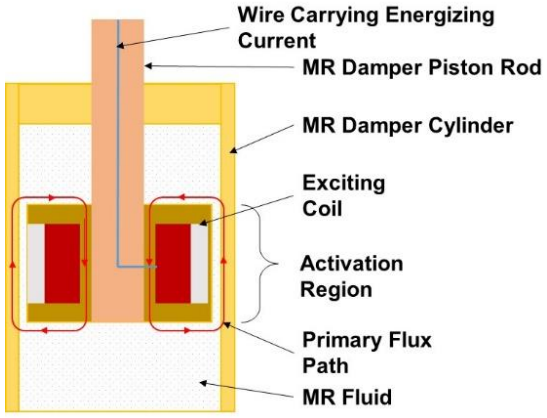

Fig. 1 Schematic and Configuration of an MR Damper

deck and hull bracing to suppress the vibration caused by sea ice and earthquake (Wu 2010). Sarrafan *et al*. (2012) numerically analyzed the performance of MR Dampers in suppressing jacket vibration due to wave-induced forces (Sarrafan *et al*. 2012). A unique application of MR Damper was done by Kang *et al*. (2013), in which MR Damper was utilized to control the stroke limit of hydro-pneumatic tensioner used for TTR (top-tensioned riser) (Kang *et al*. 2013, Kang *et al.* 2017, Kang *et al.* 2017). In the present study, the MR Damper is applied to hawser lines between two floating platforms in waves.

The implementation of MR Damper in hawser line potentially provides opportunity to regulate hawser tension due to its ability to change its damping and stiffness by electric current intensity, which can be used for hawser-tension reduction and mitigation of potential snap-loading. Therefore, this paper focuses on the effect of MR Damper on its stroke and hawser tension. A fully-coupled time-domain computer program is developed to solve the moored two-body dynamics with hawsers equipping MR Dampers. Both time histories and spectra of dynamic responses of platforms and hawser tensions and strokes and the corresponding statistical results are systematically presented and analyzed to support the MR Damper application. The effects of the pretensions on back-side assisting mooring system as well as the role of second-order wave excitations are also investigated.

2. Methods

The time-domain simulation capability with MR Dampers on hawser lines are newly developed upon existing multi-hull/riser/mooring fully-coupled in-house CHARM3D (Ran *et al*. 1996, Ran 2000, Koo 2004, Kim and Yue 1990). The CHARM3D program has been extensively validated against numerous experiments and field data (Kim 2001, Kim 2005, Yang and Kim 2009). A TLP-TAD combination is selected to represent the multibody system.

In CHARM3D, the time domain equation of motion of the vessels based on the Cummins equation (Cummins 1962) is represented as follows

$$(\mathbf{M} + \mathbf{M}_{add}(\infty))\ddot{\xi} + \mathbf{K}\xi = F_I(t) + F_c\left(t, \dot{\xi}\right) + F_M(t, \dot{\xi}) \tag{1}$$

$$F_c\left(t, \dot{\xi}\right) = -\int_0^\infty \mathbf{R}(\tau)\dot{\xi}(t-\tau)d\tau \tag{2}$$

where:
ξ is displacement,
$F_I(t)$ is total wave excitation forces, including first and second-order difference-frequency forces,
$F_M(t, \dot{\xi})$ is nonlinear drag force term from Morison's equation,
$\mathbf{M}$ is physical mass matrix,
$\mathbf{M}_{add}(\infty)$ is added mass matrix at infinite frequency,
$\mathbf{K}$ is total stiffness matrix including hydrostatic stiffness and coupling stiffness between components,
F_c is the radiation damping force, and
$\mathbf{R}$ is retardation function, which is the Fourier cosine transform of frequency-dependent radiation damping $\mathbf{C}(\omega)$ where $\mathbf{R}(t) = \frac{2}{\pi}\int_0^\infty \mathbf{C}(\omega)\frac{\cos(\omega)}{\omega}d\omega$ (Jin 2020)

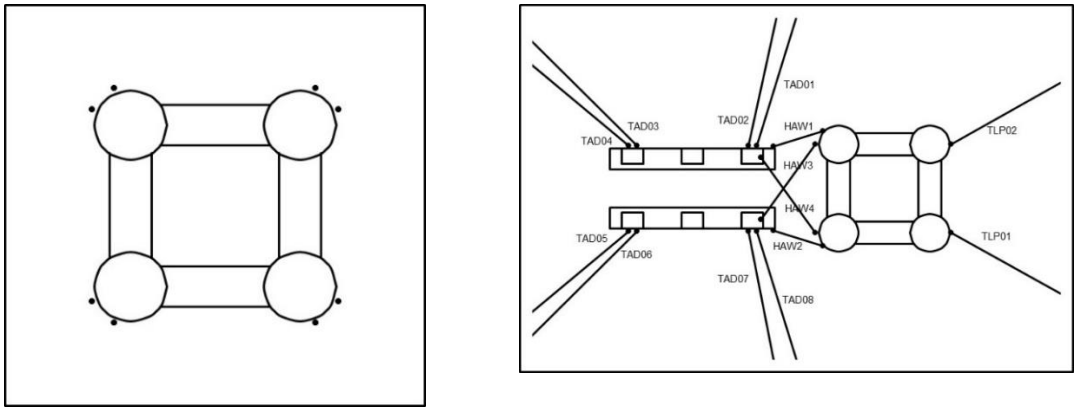

(a) (b)

Fig. 2 (a) Layout of the TLP with Tendon Hang-Off Points (2 at Each Corner) (b) and Overall System of TLP-TAD with Mooring and Hawser Lines (Tendon Hang-Off Points and Risers are not Shown)

There are 12 degrees of freedom since each platform has 6 DOFs (i.e., surge, sway, heave, roll, pitch and yaw). Frequency-domain computation is first conducted by 3D potential theory BEM (boundary element method) program to obtain frequency-dependent hydrodynamic coefficients and wave forces, which is then employed in the ensuing time-domain simulation to solve the above time-domain equation of motion. Fig. 2 shows the overall system of the TLP-TAD pair. For convenience, risers are not plotted in the figure although they are included in the coupled time-domain simulations.

The mooring, tendon, riser, and hawser systems (or line elements) are modeled by nonlinear finite rod element method. Spring and damper elements are used to connect the line elements to the vessels. The Adams-Moulton implicit method is combined with the Adams-Bashforth method for time integration of Eq. (1), which requires no iteration within the single time step. More detailed explanations for the numerical methods, including floating-body dynamics, line dynamics, floater-line interactions, can be found in Ran's dissertation (Ran 2000).

2.1 TLP-TAD system

The TLP-TAD system is a drilling system with the ability of early production and dynamic positioning. Two hold-back mooring lines are hooked up onto the TLP. Four hawser lines link the TLP and TAD together. The TLP is a conventional 4 columns and 4 pontoons TLP (see Fig. 2). Major TLP parameters are tabulated in Table 1.

The TAD vessel is a 6-columns 2-pontoons semi-submersible. 4 hawser lines link the TLP and TAD together: 2 surge hawser lines (dubbed Hawser 1 (HAW1) and Hawser 2 (HAW2)) and 2 cross hawser lines (dubbed Hawser 3 (HAW3) and Hawser 4 (HAW4)) (see Fig. 2(b)). The tensions in hawser lines are affected by TLP and TAD motions, mainly by relative surge motions considering the hawser configuration. When the two vessels move away from each other, the tension increases, and vice versa.

The mooring line configuration is shown in Fig. 3. It consists of (going from bottom to top) chain, polyester, chain and wire. The materials are shown in Table 2. There are also 24 TTRs (top tensioned risers) connected to the TLP, which were included in the numerical modeling but are not shown in Fig. 2.

Table 1 Major Parameters of the TLP (Ravikiran *et al*. 2018)

Parameters	Values
Water Depth	486 m
Draft	22.25 m
Column Diameter	22.25 m
Column Spacing	51.91 m
Column Height	35.50 m
Pontoon Width	12.93 m
Pontoon Height	8.75 m
Pontoon Length	29.41 m
Total Displacement (in-place)	50,903 mT
Number of Tendons	8
Number of Tendons at Each Column	2
Number of Risers	24

Table 2 Mooring Line Material Details (Ravikiran *et al*. 2018)

Material	Nominal Diameter	Dry Weight	Wet Weight	MBL
Wire	79 mm	35.6 kg/m	26.3 kg/m	522 MT
Chain	76 mm	115.8 kg/m	100.6 kg/m	611 MT
Polyester	-	12.9 kg/m	3.1 kg/m	587 MT

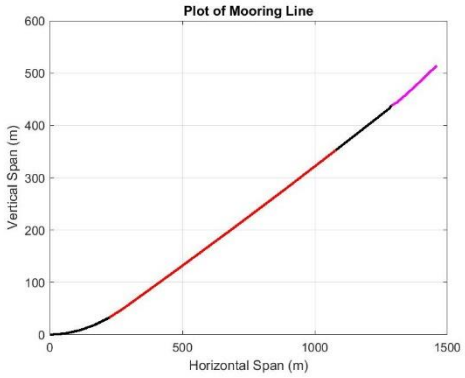

Fig. 3 Plot of Typical Mooring Line in the TLP-TAD System. Black Segment is Chain. Red Segment is Polyester. Magenta Segment is Wire

The hydrodynamic data of the TLP-TAD system are obtained by running frequency-domain multibody WAMIT program, which is based on 3D potential theory to evaluate diffraction/radiation fluid forces. Fig. 4 illustrates TLP and TAD meshing panels. Only submerged portions of the vessels are considered in the computation. There are 6232 meshing panels on TLP, and 4538 meshing panels on TAD. A convergence test with respect to the number of panels was conducted to check the

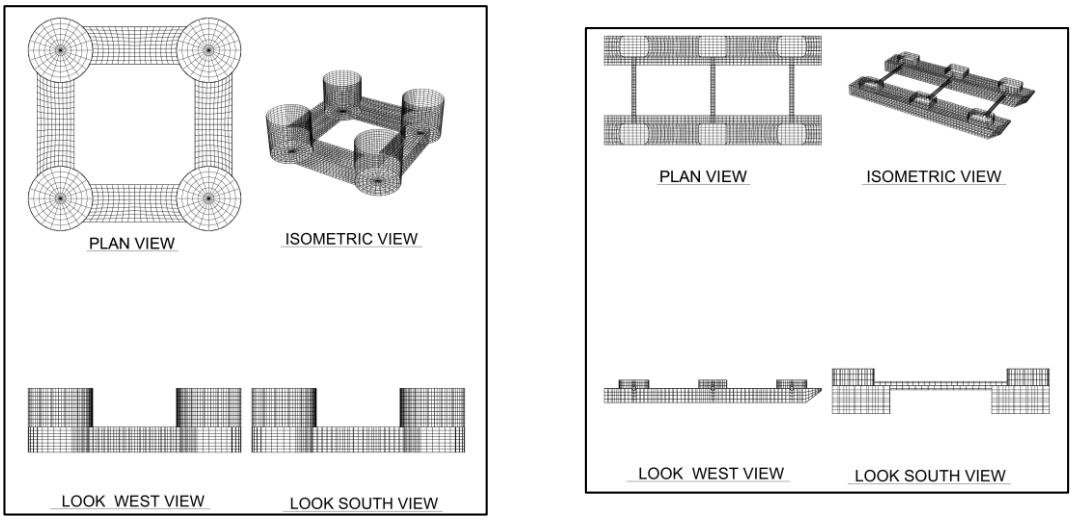

(a) (b)

Fig. 4 (a) TLP Meshing Panels and (b) TAD Meshing Panels for WAMIT Run

reliability of given results. First-order and second-order difference-frequency wave forces are computed. Newman's approximation is employed for the second-order difference-frequency force (Kim and Yue 1991), for which equivalent stiffness from tendons, mooring lines, and hawsers is incorporated into the computation.

2.2 MR damper system

Numerical MR Damper model is incorporated into CHARM3D. The model is represented by the Nonlinear Hysteretic Arctangent model (Yang *et al*. 2013, Zainuddin *et al*. 2018)

$$F_{MR\ \ Damper} = c\dot{x} + kx + \alpha \tan^{-1}\left(\beta\dot{x} + \delta sgn(x)\right) \tag{3}$$

where:

c is the viscous damping coefficient,
k is the stiffness coefficient,
α is the hysteresis factor of the MR Damper,
β and δ are the arctangent factors of the MR Damper,
x is the damper stroke, and
$\dot{x}$ is the damper stroke velocity.

$$c = 3.3 \times 10^5 i^2 + 5.5 \times 10^8 i + 2.3 \times 10^7 \tag{4}$$

$$k = 4.6 \times 10^5 i + 3.8 \times 10^4 \tag{5}$$

$$\alpha = 2.571 \times 10^6 i^2 + 4.11x10^6 + 8.0 \times 10^4 \tag{6}$$

$$\beta = 22.05i + 17.82 \tag{7}$$

$$\delta = 2.6i + 2 \tag{8}$$

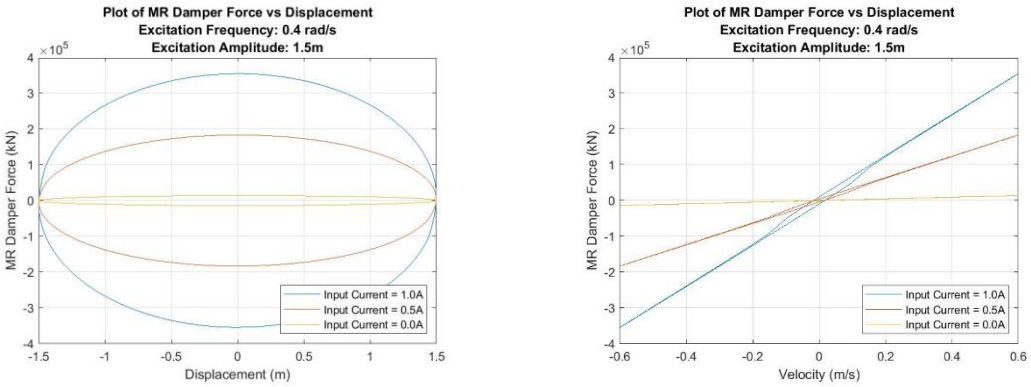

(a) (b)

Fig. 5 (a) Plot of MR Damper Force vs Displacement and (b) plot of MR Damper Force vs Velocity

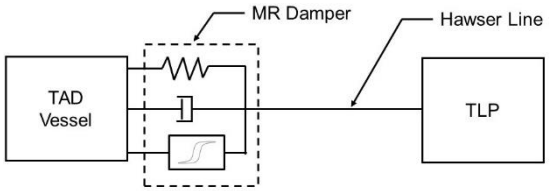

Fig. 6 Free-body Diagram of MR Damper System in a Hawser Line

i : Energizing current determined by semi-active control system.

The parameters c, k, α, β, and δ are determined from parametric studies, where the coefficients are determined to best-fit the physical MR Damper system curve while limiting MR Damper stroke to 1 m. For this particular study, a passive control of MR Damper is deployed to better understand how the MR Damper behaves under hawser loading. The passive control means that constant current is applied throughout the simulation. Three electrical currents are chosen, which are 1.0 A, 0.5 A and 0.0 A. Fig. 5 shows the MR Damper force curves against displacements and velocities for the three electrical currents.

The MR Damper system is attached at the TAD end of the hawser line. The free-body diagram is shown in Fig. 6.

The MR Damper is laid out along the hawser direction as shown in Fig. 7. This is an accurate representation of the physical MR Damper in real life i.e., MR Damper is flexible only along the tangential direction while the other two normal directions are restricted. Since the platform-line connection is modeled by the global rectangular coordinate system, there should be coordinate transformation between local (representing the MR Damper parameters) and global systems at each time step as follows

$$K_{MRg} = T^T K_{MRl} T \tag{9}$$

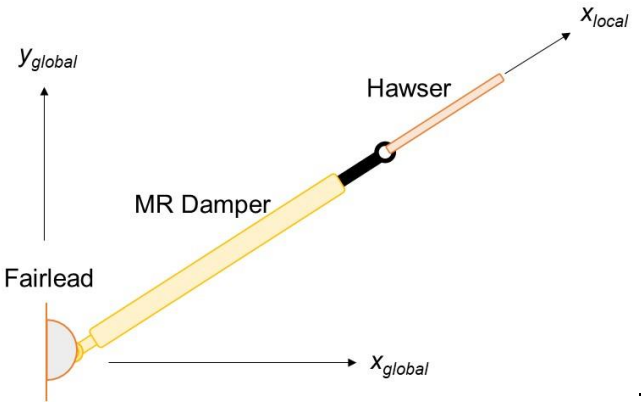

Fig. 7 Sketch of Hawser MR Damper Configuration (Not to Scale)

Table 3 Metocean Parameters

Parameters	Values
Significant Wave Height	2.1 m
Peak Period	7.0 s
Overshooting Parameter, γ	1.6
Main Direction of Waves	0 deg
Direction of Current	0 deg
Surface Current	0.56 m/s
Wind Speed at 10 m elevation	10.4 m/s

where:

T is transformation matrix from local to global ($x_{global} = T\hat{x}_{local}$),

K_{MRg} is MR Damper parameters in global axis, and

K_{MRl} is MR Damper parameters in local axis.

2.4 Metocean data

A benign sea environment (wind-wave-current) is used in the simulation. This reflects the actual operating condition of the TLP-TAD system. The environment heading is zero degree, which is in the surge direction of the system. The metocean data is tabulated in Table 3.

JONSWAP wave spectrum is used as the basis to generate the random wave. The simulated random wave time series from the given wave spectrum $S(\omega)$ can be expressed by superposition of a large number of sinusoidal wave components with random phases

$$\eta(t,x) = \sum_{i=1}^{N} A_i \cos(k_i x + \omega_i t + \varepsilon_i) = Re\left[\sum_{i=1}^{N} A_i e^{i(k_i x - \omega_i t + \varepsilon_i)}\right] \quad (10)$$

$$A_i = \sqrt{2S(\omega_i)\Delta\omega} \quad (11)$$

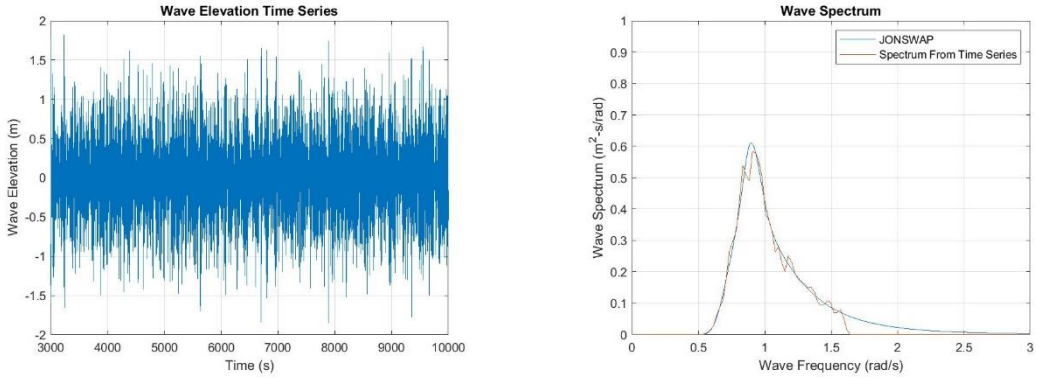

(a) (b)

Fig. 8 (a) Wave Elevation Time Series and (b) JONSWAP Wave and Recovered Spectrums

where:
A_i is wave amplitude,
k_i is wave number,
ω_i is wave frequency,
N is the number of wave components,
$\Delta\omega$ is interval of frequency division, and
ε_i is random phase uniformly distributed between 0 and 2π.

To generate long time series and avoid signal repetition of random wave, a sufficiently small $\Delta\omega$ is necessary (Ran 2000), which leads to large computing time. To avoid the increase of wave components, a modified wave elevation equation is adopted as follows (Kim and Yue 1991)

$$\eta(t,x) = Re\left[\sum_{i=1}^{N} A_i e^{i(k_i x - \omega_i' t + \varepsilon_i)}\right] \tag{12}$$

where:

$\omega_i' = \omega_i + \delta\omega_i$,

$\delta\omega_i$ is random perturbation uniformly distributed between $-\frac{\Delta\omega}{2}$ and $\frac{\Delta\omega}{2}$.

The time series of the wave and the wave spectrum are shown in Fig. 8. 3-hour simulation is conducted to guarantee that the statistical data, such as maximum, minimum, and standard deviation, are reasonable. 100 regular wave components are superposed to generate the random waves. Lower and upper cut-off frequencies were 0.5 and 1.6 rad/s, respectively, outside which little wave energy exists. The generated random wave elevation is acceptable based on the comparison between the original JONSWAP wave spectrum and re-generated spectrum from the time series (Fig. 8(b)).

2.5 Loadcase

Four cases are considered in this analysis. The first case is called Base Case where the hawser connection on TAD end is hinged at the fairlead (no MR Damper). The second, third, and fourth cases are called MR Damper cases where the hawser TAD ends are equipped with MR Dampers, and the MR Dampers are energized with 1.0 A, 0.5 A and 0.0 A electric currents, respectively. This

Table 4 MR Damper Parameters for Energizing Current 1.0 A, 0.5 A and 0.0 A

Parameters	**Energizing Current 1.0 A**	**Energizing Current 0.5 A**	**Energizing Current 0.0 A**
Damping Coefficient (c) (kN/m/s)	5.810×10^5	3.012×10^5	2.311×10^4
Stiffness Coefficient (k) (kN/m)	500.0	268.8	37.8
Hysteresis Coefficient (α) (kN)	100.00	41.08	1.18
Arctangent Coefficient (β)	39.87	28.85	17.82
Damping Coefficient (δ)	4.9	3.6	2.3

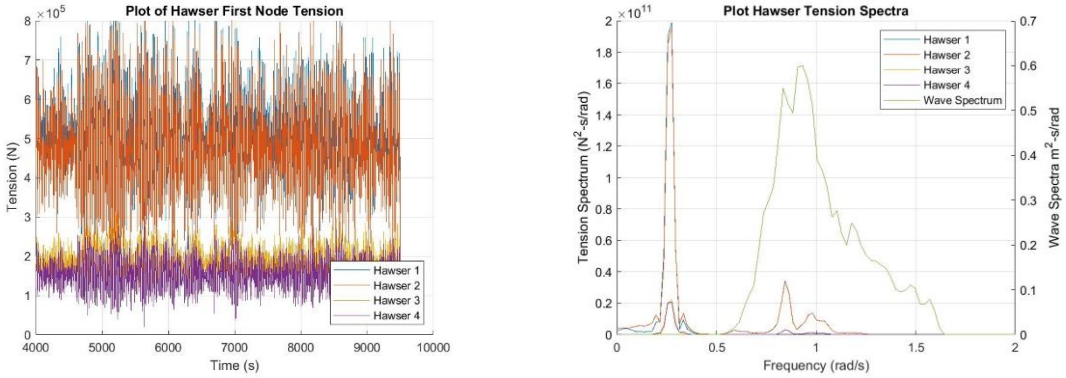

(a) (b)

Fig. 9 Base Case's Tension Time Series (a) and Spectra (b) of Hawser First Node

is to examine the effect of introducing variable MR stiffness/damping into the hawser line. Table summarizes the MR Damper parameters for the aforementioned cases.

3. Results and discussion

3.1 Hawser tension fluctuation

As mentioned before, hawser tension fluctuation is mainly due to the relative TLP-TAD surge motion. Understanding this is important before discussing the role of MR Damper to lower the tension. Fig. 9 shows the hawser-first-node tension fluctuation for Base Case. First node is the node connected to the TLP fairlead and its tension is called hawser tension from now on. Hawser 1 and Hawser 2 have higher tensions than Hawser 3 and Hawser 4. This is because Hawser 1 and Hawser 2 are oriented along the environment direction (surge) hence receiving more loading due to prevalent vessel motions in surge direction. Hawser 3 and Hawser 4 are oriented in surge-sway direction, to better restrict sway-side motions in oblique waves. Another thing to note is the mixture of high and low frequency tension fluctuations, a similar trend to the relative surge motion as shown in Fig. 10.

Fig. 10(a) shows the zoomed time series of TLP and TAD surge motions to illustrate the out-of-phase surge motions between the TLP and TAD. Even with the high initial mean tension between

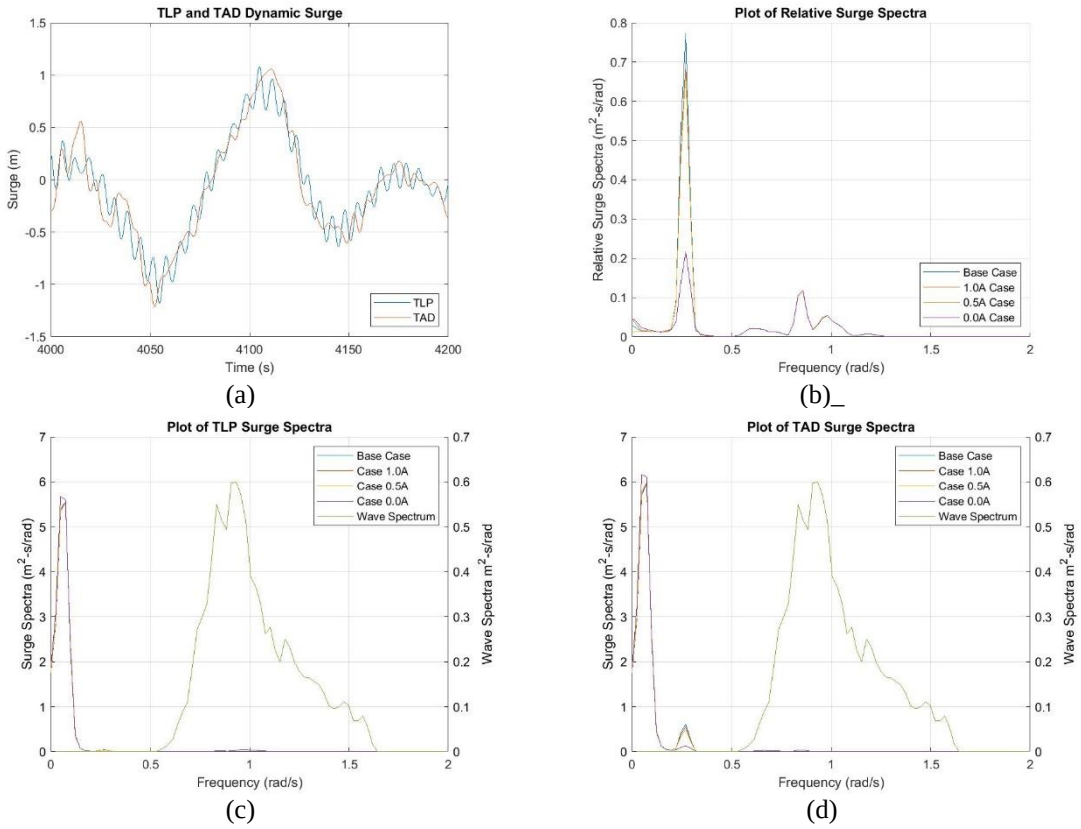

Fig. 10 (a) Base Case's Dynamic Surge Motions and (b) Relative Surge Motion Spectra of TLP and TAD, (c) TLP surge spectra, (d) TAD surge spectra. For comparison, the cases with electrical currents are also given in (b),(c),(d)

the TLP and TAD, their surge motions are not entirely in phase. This is due to the fact that the two vessels have different station-keeping methods i.e., TLP with a combination of tendons (vertical mooring) and taut assisting mooring lines backward and TAD with entirely spread mooring lines. Therefore, the surge stiffness of the two vessels is different, leading to differences in the surge dynamic motion characteristics. In general, similar slow-varying motions are observed in both TLP and TAD, whereas non-synchronous motions at the TAD surge natural frequency (~0.25 rad/s) cause the corresponding hawser's dynamic tension there. The slowly-varying surge motions at less than 1.0 rad/s are large (Figs. 10(c) and 10(d)) but they tend to be more synchronous, and thus their contributions to the low-frequency tensions are unimportant. The hawser tension spectra demonstrate the correlation between hawser tension and relative surge motion in which the tension's frequency range coincides with that of relative surge motion, as in Figs. 9(b) and 10(b).

The relative surge motions consist of three frequency components; lowest surge natural frequency of TLP (around 0.08 rad/s), surge resonance frequency of TAD (around 0.25 rad/s), and wave frequency components. The wave frequency motions are not affected by the MR Damper. However, the low-frequency relative surge motions are related to resonant surge responses and they can be mitigated by introducing MR Damper through controlling the axial stroking rate and speed

Table 5 TLP-TAD Relative Surge

Parameters	Relative Surge			
	Base Case	MR Damper Case (1.0A Input Current)	MR Damper Case (0.5A Input Current)	MR Damper Case (0.0A Input Current)
Mean (m)	1.15	1.86	2.62	8.82
Max (m)	2.35	3.04	3.77	9.75
Min (m)	0.21	0.96	1.77	8.15
Std. Dev.	0.26	0.26	0.25	0.19

with changing the input electric current. Table 5 shows the statistics of the relative surge motions for various MR-Damper conditions. When MR Damper is introduced instead of pin-joint, the mean relative surge (related to mean MR Damper stroke) is increased, but the dynamic relative surge motions are reduced, which results in the corresponding reduction of hawser tension. The significant increase of mean stroke is directly related to the MR-Damper length, so it can be problematic in view of practicality. One potential solution is to introduce an additional parallel mechanical spring to limit the mean stroke. This will further be discussed in the following sections.

3.2 Results from Implementation of MR damper

Table 6 shows the mean, maximum, and minimum tensions of the hawser lines with the implementation of MR Damper. Reductions in mean and maximum tensions can be seen in Hawser 1 and Hawser 2. This is expected since the TAD end connection is more flexible with MR Dampers than typical pin joints. This also means that the resonant out-of-phase relative surge motions of the vessels are accommodated by the MR Damper stroke. Smaller currents lead to smaller tensions. However, smaller currents cause larger mean stroke (larger relative mean surge), leading to lower hold back mooring tension. The lower hold back mooring tension reduces the coupling of surge motion between the TLP and TAD. This leads to lower pulling force between the two floaters, hence lower hawser tension. The cross hawsers (Hawser 3 and Hawser 4) are also impacted but with lesser degree. Among MR Damper cases, the reductions of mean and maximum tensions are inline with the reductions in input currents. This is expected since the MR Damper resistance is smaller in lower electric current. There are also reductions in tension range (maximum tension minus minimum tension) in the MR Damper cases, which is promising for tension mitigation.

On the other hand, Hawser 3 and Hawser 4 see slight increments in mean and maximum tensions with the implementation of MR Damper, although reductions are also seen with lower input current for the same reason mentioned above. The increments of hawser tension with MR Damper can be explained by the shift of load from Hawser 1 and Hawser 2 to Hawser 3 and Hawser 4, as Hawser 1 and Hawser 2 take less load (tension). This shift of loads is actually beneficial since the Hawser 3 and Hawser 4 tensions are much smaller than Hawser 1 and Hawser 2 tensions. Hawser 3 and Hawser 4 MR Dampers are laid in surge-sway orientation (see Fig. 2(b)), so they are to contribute more in the case of oblique incident waves.

Note that in all MR Damper cases, the electric currents remain the same. A fine tune of MR Damper input current via semi-active control can be applied to reduce the maximum hawser tension among the respective hawsers, which will be the subject of the next study.

Table 6 (a) First Node's Tensions in Hawser 1 and Hawser 2 and (b) in Hawser 3 and Hawser 4

(a)

Parameters	Hawser 1				Hawser 2			
	Base Case	MR Damper Case (1.0 A Input Current)	MR Damper Case (0.5 A Input Current)	MR Damper Case (0.0 A Input Current)	Base Case	MR Damper Case (1.0 A Input Current)	MR Damper Case (0.5 A Input Current)	MR Damper Case (0.0 A Input Current)
Mean Tension (kN)	505.76	461.14	437.14	293.81	483.87	442.14	420.00	286.38
Max Tension (kN)	1039.33	981.72	944.80	702.75	1027.84	971.89	934.34	683.47
Min Tension (kN)	132.13	106.39	102.92	30.76	70.82	47.27	45.38	27.36
RMS Tension	520.46	476.19	452.09	306.38	499.71	458.44	436.25	300.64
Std. Dev.	122.87	118.80	115.30	86.86	124.87	121.20	117.99	91.51
Delta Tension (kN)	907.20	875.32	841.88	671.99	957.02	924.62	888.96	656.11

(b)

Parameters	Hawser 3				Hawser 4			
	Base Case	MR Damper Case (1.0 A Input Current)	MR Damper Case (0.5 A Input Current)	MR Damper Case (0.0 A Input Current)	Base Case	MR Damper Case (1.0 A Input Current)	MR Damper Case (0.5 A Input Current)	MR Damper Case (0.0 A Input Current)
Mean Tension (kN)	186.02	224.73	226.93	188.71	154.23	195.10	198.91	173.03
Max Tension (kN)	347.42	384.55	384.37	333.28	337.38	377.57	379.77	331.59
Min Tension (kN)	58.40	100.57	107.62	89.06	20.28	62.10	69.05	57.75
RMS Tension	190.18	228.06	230.09	191.07	159.32	199.05	202.68	176.29
Std. Dev.	39.60	38.82	38.03	29.94	39.95	39.43	38.92	33.74
Delta Tension (kN)	289.02	283.98	276.76	244.22	317.10	315.47	310.72	273.84

Figs. 11 and 12 show the hawser first-node tension time series and spectra for varying electric currents. The tension fluctuations exhibit both high and low-frequency components for the same reason discussed in Base Case tension fluctuation above. A significant reduction in tensions is observed at 0.0 A; however, it still maintains positive mean tension to avoid any snap response (sudden loose-to-tight) and snap tension. Corresponding spectra are presented in Fig. 12. There exist appreciable differences only at TAD resonance frequency (0.25 rad/s) with varying electric current.

The corresponding dynamic tension decreases with decreasing electric current by the same reason as discussed above. The trend is very similar to that of relative surge motion (Fig. 10(b)) indicating that the dynamic tension is directly influenced by the vessels' surge relative displacement.

Considering the noticeable reduction with reduced current intensity in above examples, more work by MR Damper control is possible i.e., when the tension with 1 A reaches a certain limit, the current can be reduced to make the MR Damper softer so that the instantaneous tension may be reduced. This is similar to the traditional winch control i.e., the length is temporarily increased to reduce the instantaneous tension. However, this current reduction can result in the increased stroke. Therefore, it has to be only during a very short time interval. Table 7 summarizes the statistics of MR Damper stroke for various electric currents. It is seen that the mean stroke is too large when

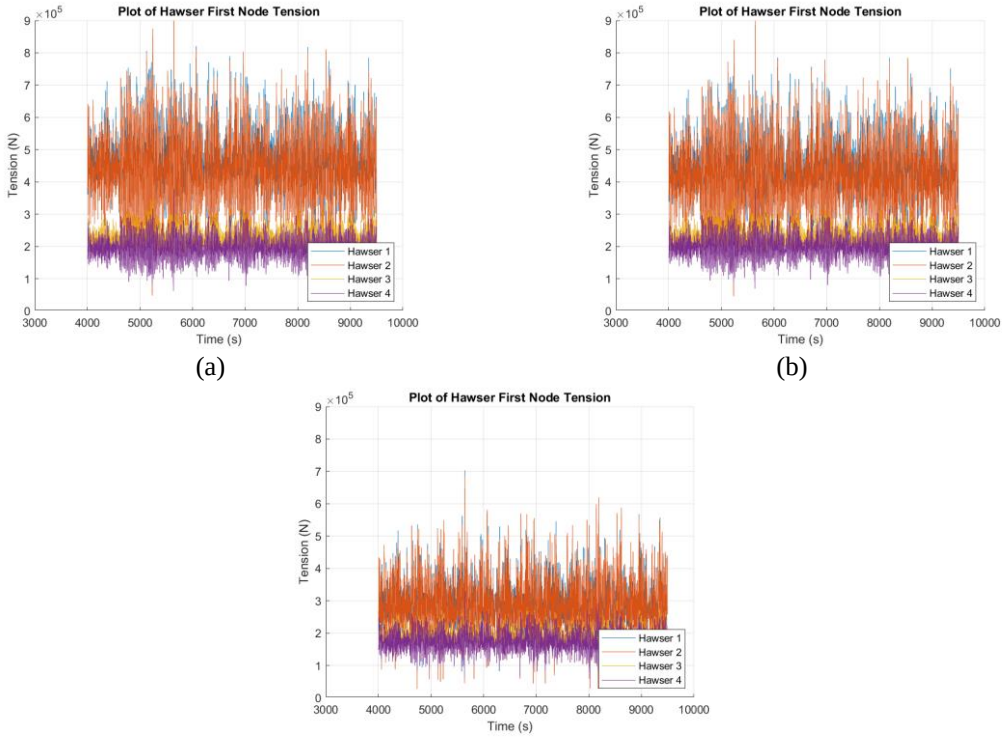

Fig. 11 Tension of Hawser's First Node with MR Damper in (a) Case 1.0 A, (b) Case 0.5 A and (c) Case 0.0 A

electric current is close to zero, which is practically not acceptable. In this case, a remedy by employing additional parallel mechanical spring needs to be considered. The stroke dynamic fluctuation is not that significant especially when the electric current is increased, as illustrated in Fig. 13, since the hawser lines then remain tight with high mean tension so that the two floaters move together as much as possible. The mean stroke should also be limited by the length of the connection bridge, which is fixed at one floater and free to move on the other floater.

Note that the stroke's mean value increases as the damper input current decreases, indicating the damper resistance decreases in accordance with the decrease in input current. This relationship between MR Damper current and MR Damper stroke is nonlinear. As for MR Damper Case 0.0 A, the mean stroke is significantly large compared to higher current cases. This is the setback for the decrease in hawser tension in lower current. Further studies taking advantage of the decrease of hawser tension at 0.0 A whilst maintaining lower MR Damper stroke by additional parallel mechanical spring or implementing semi-active control with varying input current will be considered.

Next, let us consider whether the variation of stroke for the various MR Damper currents affects the vessel motions, especially the surge motions. Table 8 shows the surge motions of the TLP and TAD. The introduction of different MR Damper currents little influences the dynamic surge motion of each vessel judging from the standard deviations. On the other hand, the mean surge offsets of TAD are changed according to the increase in mean stroke, which can intuitively be expected. This.

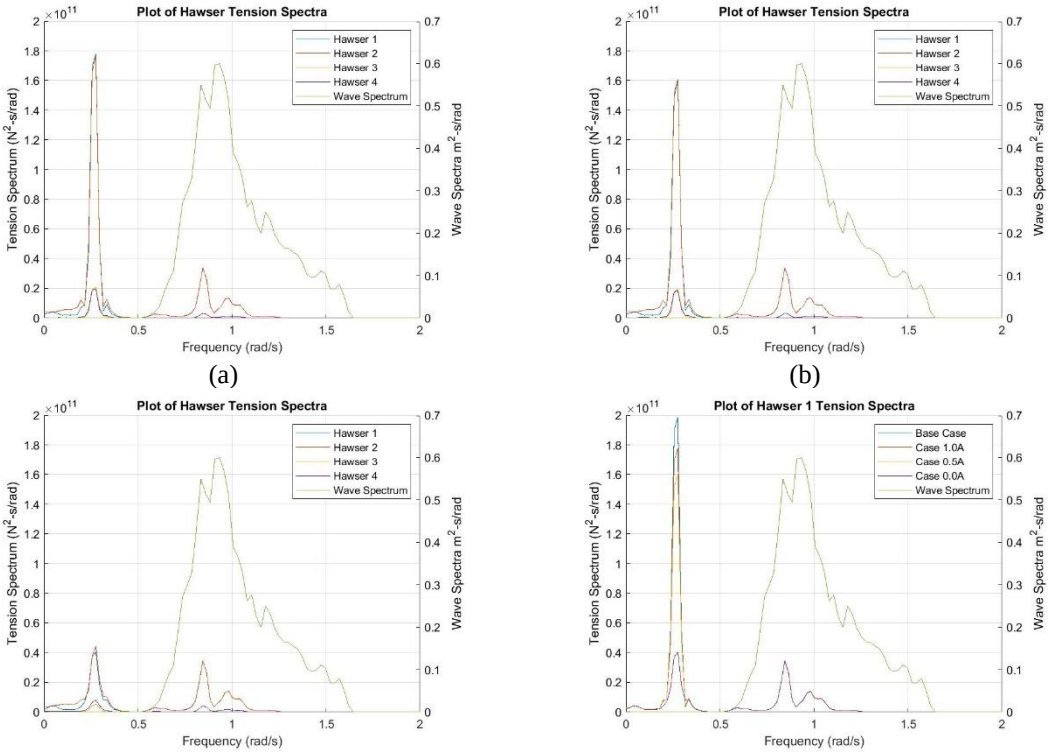

Fig. 12 Tension Spectra with MR Damper in (a) Case 1.0A, (b) Case 0.5 A, (c) Case 0.0 A, and (d) Hawser 1 Tension Spectra

Table 7 MR Damper's Stroke in Hawser 1–4

Parameters	Hawser 1			Hawser 2		
	MR Damper Case (1.0 A Input Current)	MR Damper Case (0.5 A Input Current)	MR Damper Case (0.0 A Input Current)	MR Damper Case (1.0 A Input Current)	MR Damper Case (0.5 A Input Current)	MR Damper Case (0.0 A Input Current)
Mean Stroke (m)	0.79	1.57	7.91	0.75	1.50	7.70
Max Stroke (m)	0.80	1.59	8.02	0.76	1.52	7.83
Min Stroke (m)	0.77	1.55	7.83	0.73	1.48	7.58
RMS Stroke	0.79	1.57	7.91	0.75	1.50	7.70
Std. Dev.	0.00	0.01	0.03	0.01	0.01	0.04
Parameters	**Hawser 3**			**Hawser 4**		
	MR Damper Case (1.0 A Input Current)	MR Damper Case (0.5 A Input Current)	MR Damper Case (0.0 A Input Current)	MR Damper Case (1.0 A Input Current)	MR Damper Case (0.5 A Input Current)	MR Damper Case (0.0 A Input Current)
Mean Stroke (m)	0.29	0.74	4.95	0.23	0.64	4.53
Max Stroke (m)	0.29	0.75	4.99	0.23	0.64	4.59
Min Stroke (m)	0.28	0.73	4.91	0.22	0.62	4.47
RMS Stroke	0.29	0.74	4.95	0.23	0.64	4.53
Std. Dev.	0.00	0.00	0.01	0.00	0.00	0.02

Table 8 Surge Motion of TLP and TAD

Parameter	TLP Surge			
	Base Case	**MR Damper Case (1.0 A Input Current)**	**MR Damper Case (0.5 A Input Current)**	**MR Damper Case (0.0 A Input Current)**
Mean (m)	3.92	3.82	3.72	2.93
Max (m)	6.47	6.38	6.28	5.51
Min (m)	1.81	1.70	1.59	0.74
RMS	3.98	3.88	3.78	3.00
Std. Dev.	0.67	0.67	0.67	0.67
Parameters	**TAD Surge**			
	Base Case	**MR Damper Case (1.0 A Input Current)**	**MR Damper Case (0.5 A Input Current)**	**MR Damper Case (0.0 A Input Current)**
Mean (m)	5.07	5.69	6.34	11.75
Max (m)	7.77	8.37	9.02	14.44
Min (m)	2.69	3.31	3.96	9.46
RMS	5.12	5.73	6.38	11.78
Std. Dev.	0.71	0.71	0.71	0.71

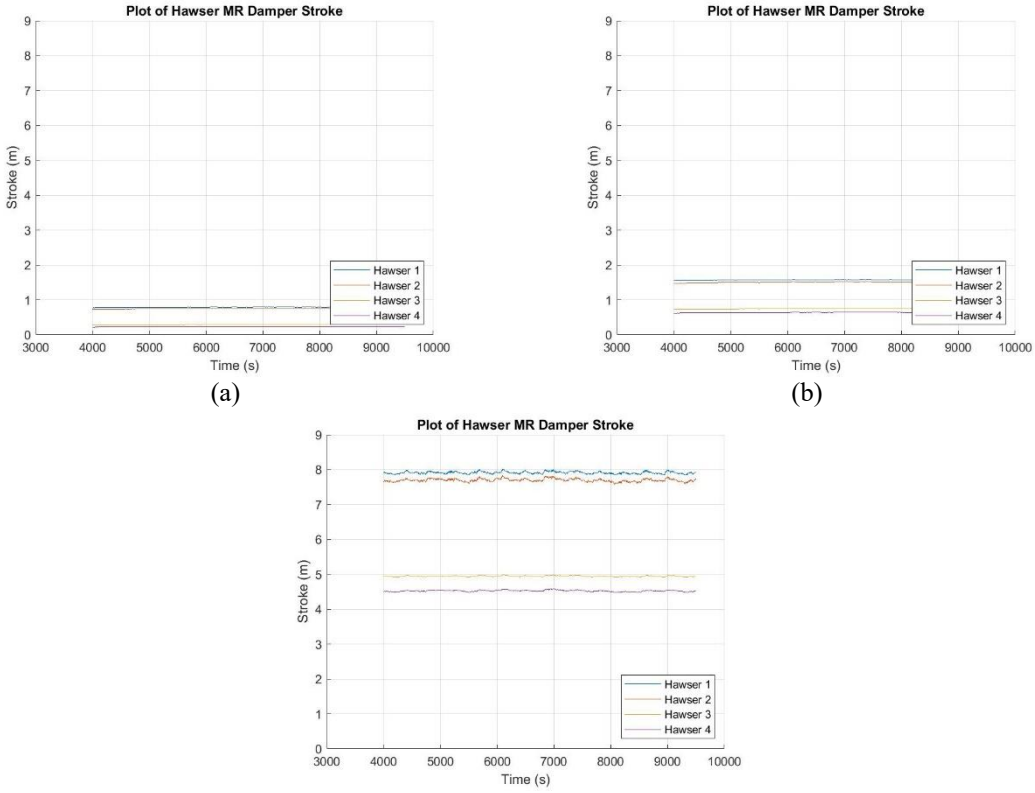

Fig. 13 Stroke with MR Damper in (a) Case 1.0 A, (b) Case 0.5 A, and (c) Case 0.0 A

means that the dynamic characteristics of each platform remain almost the same regardless of the change of electric currents in MR Damper. As was seen before, in the case of 0 A case, we have the largest maximum minus minimum surges both for TLP and TAD.

The effect of low input current in hawser tension and the effect of high input current in stroke can be capitalized further through the implementation of semi-active control system. Semi-active control system can be deployed to regulate hawser tension to keep it below a certain threshold and to keep dynamic tension within the snap tension limit. The control strategy is to relax the MR Damper when the hawser tension increase beyond a predetermined upper threshold and to stiffen MR Damper when the hawser tension decrease below a predetermined lower threshold. Based on this strategy, few control systems can be utilized, such as Skyhook Control and Fuzzy-Logic Control.

3.3 Effects of lower mooring pretension

The initially large static tension in the Hawser 1 and Hawser 2 was caused by high pretension of back-side mooring. The initial large hawser static tension was intended so that the TLP and TAD may move synchronously as more like a connected rigid body to minimize their relative surge motion, which results in minimizing the movement of connection bridge too. However, it caused a large initial stroke of MR Damper without electric current and made its application and control less straightforward. In this regard, we want to investigate the effect of reducing back-side mooring pretension by increasing hawser length for the same system set up of Base Case. In that regard, the length of Hawser 1 and Hawser 2 was increased by 8 m, and Hawser 3 and Hawser 4 by 5.1 m. Then the pretensions of the backside mooring are reduced and the redistribution of the initial mooring tension is shown in Fig. 14. The corresponding tension statistics for the same environmental loads are given in Table 9. Both static and dynamic tensions of hawser 1-2 are significantly reduced. The reduction rates of sideway hawsers 3-4 are much smaller but it is still beneficial. The reduced static tension will accordingly reduce the initial stroke of MR Damper, which implies much easier application of MR Damper and its control. Therefore, when MR Damper is to be introduced in the TLP-TAD hawser system, the optimization including the initial pretension of the whole mooring-hawser system needs to be considered.

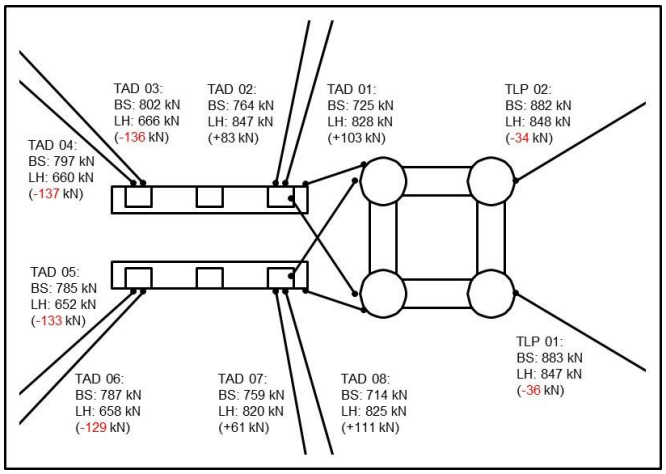

Fig. 14 Mooring Pretension Comparison between Base Case (BS) and Longer Hawser Case (LH)

Table 9 Hawser Tension Comparison between Base Case and Longer Hawser Case

Parameters	Hawser 1		Hawser 2		Hawser 3		Hawser 4	
	Base Case	Longer Hawser	Base Case	Longer Hawser	Base Case	Longer Hawser	Base Case	Longer Hawser
Mean Tension (kN)	505.76	316.64	483.87	295.91	186.02	161.26	154.23	127.21
Max Tension (kN)	1039.33	755.73	1027.84	708.80	347.42	324.45	337.38	320.64
Min Tension (kN)	132.13	0.16	70.82	-1.36	58.40	32.16	20.28	0.10
RMS Tension	520.46	331.39	499.71	312.37	190.18	166.47	159.32	134.18
Std. Dev.	122.87	97.77	124.87	100.06	39.60	41.33	39.95	42.69

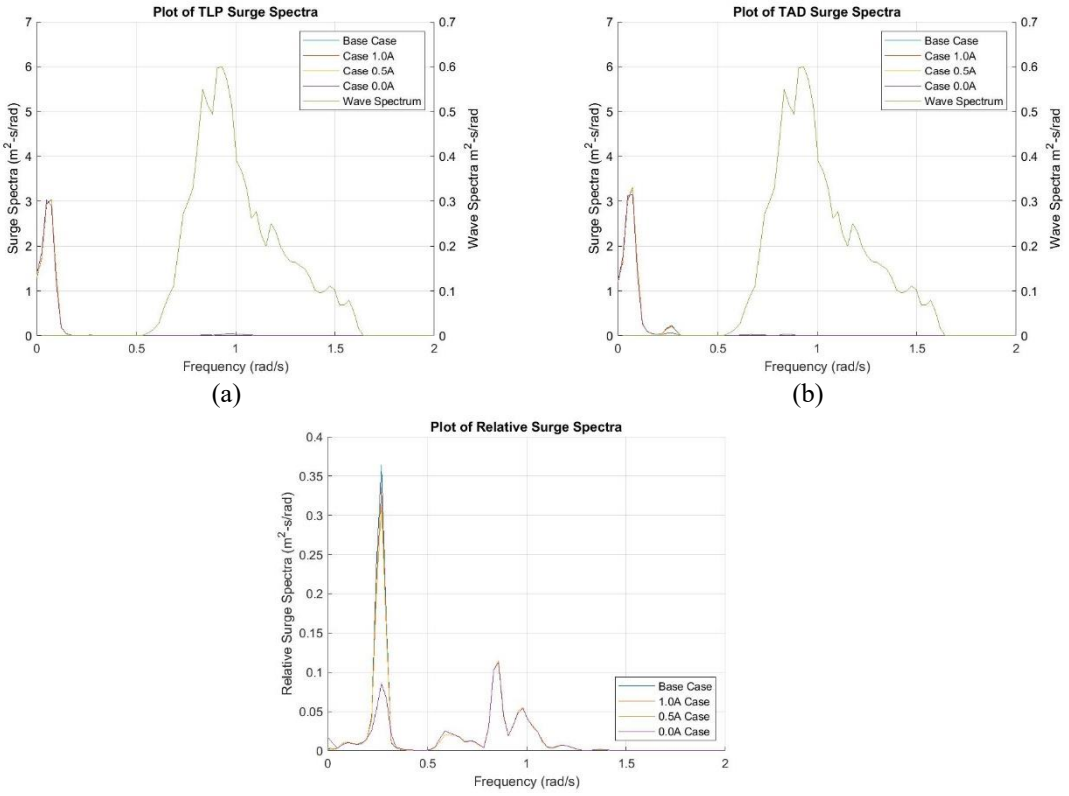

Fig. 15 Case without second-order force: (a) TLP Surge Spectra, (b) TAD Surge Spectra, and (c) Relative Surge Spectra

3.4 Effects of excluding second-order wave force and viscous force in the basic case

Lastly, the effects of including second-order difference-frequency wave forces and the corresponding slowly varying surge motions are discussed here. In this regard, the Base Case excluding second-order wave force is shown in Fig. 15 so that it can be compared to Fig. 10. As expected, the slowly-varying surge responses are significantly (about 50%) reduced after excluding the second-order wave forces. It is also seen that MR Damper is not effective for steady-state wave-

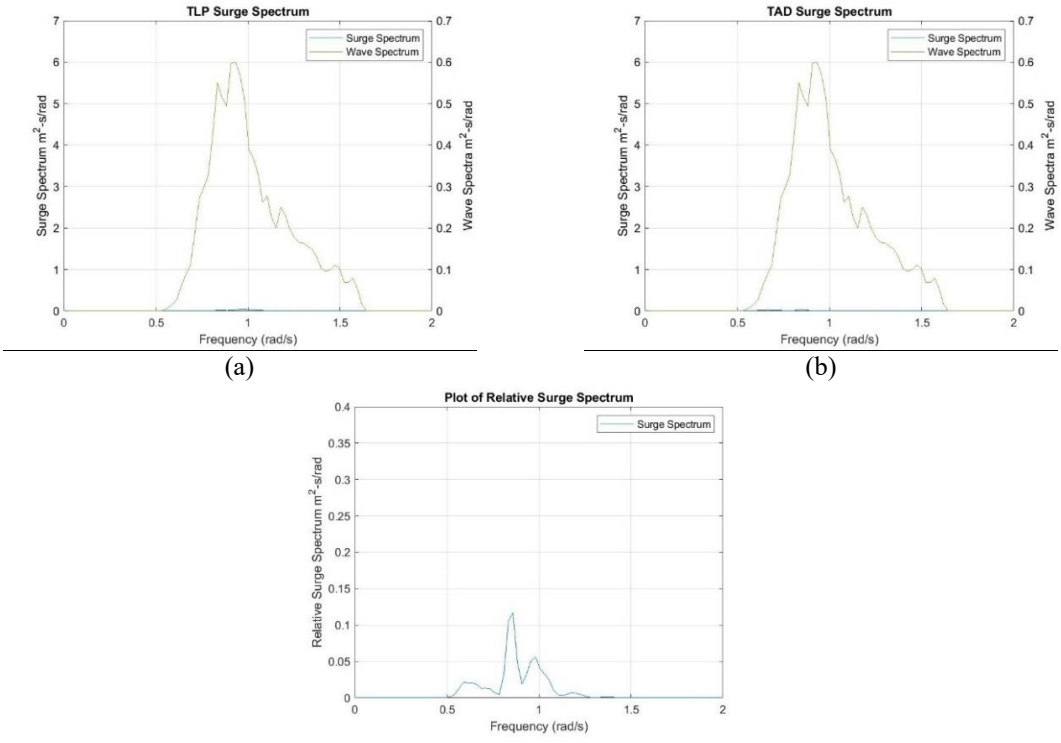

Fig. 16 Case Without Second-order Wave Force, Wind Loading, and Vessel Drag Force: (a) TLP Surge Spectra, (b) TAD Surge Spectra, and (c) Relative Surge Spectra

frequency responses but works on resonant low-frequency responses. Therefore, the inclusion of the second-order wave effects is essential in the MR Damper design and control. Fig. 15 also shows that there still exist excitations/responses in the low frequency region even after excluding the second-order wave force. It is due to the slowly-varying wind forces and viscous drag forces. There are two sources of viscous forces in the system. The first source is the vessel drag force implemented through vessel Morison member. The second source is the Morison force on the legs (tendons, risers, and moorings) which is the result of current action. Fig. 16 shows vessel surge spectra without second-order wave force, wind loading, and vessel drag forces. From the plot, one can see that the low frequency excitations/responses almost disappear, as expected. The remaining very small low-frequency excitations/responses are due to the wave-current-induced drag forces on the legs.

4. Conclusions

MR Damper in TLP-TAD hawser system was simulated using the in-house multi-hull-riser-mooring-hawser fully coupled dynamic simulation program CHARM3D with MR Damper numerical module incorporated into it in time domain. Only the TAD ends of the hawsers are equipped with MR Dampers. A 3-hour benign storm (wind-wave-current) was used as an environmental condition. Four hawser cases were run, namely Base Case (pin joints at both fairlead

connections) and three MR Damper cases at TAD connection with three different electric currents (1.0 A, 0.5 A and 0.0 A).

The introduction of MR Damper led to a reduction in Hawser 1 and Hawser 2 mean and maximum tensions by reducing the resonant TLP-TAD relative surge motion near TAD surge natural frequency with accommodating MR Damper. However, such effect was not seen in Hawser 3 and Hawser 4 maximum tensions, although they are much smaller compared to those of Hawser 1 and Hawser 2, due to load redistribution. The stroke of MR Damper increased as the input electric current decreased indicating less MR Damper resistance in lower input current. There was less surge coupling between the TLP and TAD with the introduction of MR Damper since MR Damper stroke accommodated the out-of-phase motions between the two vessels. Since the mean stroke of the MR Damper with minimal current is too large, either additional parallel mechanic spring or less initial hawser pretension needs to be considered. The wave frequency components of tensions and strokes were not affected by changing the MR damping.

The increases of hawser length reduce the back-side mooring pretension, leading to lower mean and dynamic tensions of the hawser lines. Hence, when MR Damper for hawser is employed, it needs to be coordinated with mooring system design. The second-order wave force, wind loading, and viscous force lead to low-frequency surge excitations/responses, and they are closely correlated with MR Damper application for hawser lines.

Future work includes developing the control system of the MR Damper to take advantage of the MR Damper's abilities to varying its parameters. The objective is to decrease the maximum tension and tension range further, whilst maintaining the stroke to be less than 1 m.

Acknowledgments

The author would like to acknowledge Shell for providing the guidance on practical application of this work to the industry realistic issues. This work was also partly supported by the National Research Foundation of Korea (NRF) grant funded by the Korea government (MSIT) (No. 2017R1A5A1014883).

References

Bitaraf, M., Ozbulut, O.E., Hurlebaus, S. and Barroso, L. (2009), "Application of semi-active control strategies for seismic protection of buildings with MR dampers", *Eng. Struct.*, **32**(10), 3040-3041. https://doi.org/10.1016/j.engstruct.2010.05.023.

Cummins, W.E. (1962), "The impulse response function and ship motions", *Symposium on Ship Theory*, Hamburg.

Jin, C., Kang, H., Kim, M. and Bakti, F.P. (2020), "Performance evaluation of surface riding wave energy converter with linear electric generator", *Ocean Eng.*, **218**, 1-16. https://doi.org/10.1016/j.oceaneng.2020.108141.

Kang, H.S. (2015), *Semi-Active Magneto-Rheological Damper and Applications in Tension Leg Platform/Semi-Submersible,* College Station, Texas: Texas A&M University.

Kang, H.S., Kim, M.H. and Bhat, S. (2017), "Tension variations of hydro-pneumatic riser tensioner and implications for dry-tree interface in semisubmersible", *Ocean Syst. Eng.*, **7**(1), 21-38. https://doi.org/10.12989/ose.2017.7.1.021.

Kang, H.S.,. Kim, M.H., Bhat, S. and Kang, H.Y. (2013), "Semi-active magneto-rheological damper to reduce the dynamic response of top-tension risers", *International Society of Offshore and Polar Engineers (ISOPE)*, Anchorage.

Kim, M.H. and Yue, D.K.P. (1990), "The complete second-order diffraction solution for an axisymmetric body Part 2. bichromatic incident waves and body motions", *J. Fluid Mech*., **211**, 557-593. https://doi.org/10.1017/S0022112090001690.

Kim, M.H. and Yue, K.P. (1991), "Sum- and difference-frequency wave loads on a body in unidirectional Gaussian seas", *J. Ship Res*,, **35**(2), 127-140. https://doi.org/10.5957/jsr.1991.35.2.127.

Kim, M.H., Koo, B.J., Mercier, R.M. and Ward, E.G. (2005), "Vessel/mooring/riser coupled dynamic analysis of a turret-moored FPSO compared with OTRC experiment", *Ocean Eng*., **32**(14-15), 1780-1802. https://doi.org/10.1016/j.oceaneng.2004.12.013.

Kim, M.H., Ran, Z. and Zheng, W. (2001), "Hull/mooring coupled dynamic analysis of a truss spar in time domain", *Int. J. Offshore Polar Eng*., **11**(1), 42-54.

Koo, B.J., Kim, M.H. and Randall, R.E. (2004), "The effect of nonlinear multi-contact coupling with gap between risers and guide frames on global spar motion analysis", *Ocean Eng*., **31**(11-12), 1469-1502. https://doi.org/10.1016/j.oceaneng.2004.01.002.

Krenk, S. (2000), "Vibrations of a taut cable with an external damper", *J. Appl. Mech.*, **67**(4), 772-776. https://doi.org/10.1115/1.1322037.

Main, J.A. and Jones, N.P. (2007), "Vibration of tensioned beams with intermediate damper. I: Formulation, influence of damper location", *J. Eng.Mech*., **133**(4), 1-10. https://doi.org/10.1061/(ASCE)0733-9399(2007)133:4(369).

Ran, Z. (2000), *Coupled Dynamic Analysis of Floating Structures in Waves and Currents,* College Station, Texas: Texas A&M University.

Ran, Z., Kim, M.H., Niedzwecki, J.M. and Johnson, R.P. (1996), "Response of a spar platform in random waves and currents (Experiment vs. Theory)", *Int. J. Offshore Polar.*, **6**(1), 27-34.

Ravikiran, K., Amurol, S. and Tan, H. (2018), "Design and operation of coupled mooring system for tender-assisted drilling at Malikai TLP", *Proceedings of the Offshore Technology Conference*, Houston.

Sarrafan, A., Zareh, S.H., Khayyat, A.A.A. and Zabihollah, A. (2012), "Neuro-fuzzy control strategy for an offshore steel jacket platform subjected to wave-induced forces using magnetorheological dampers", *Mech. Sci. Technol*., **26**(4), 1179-1196. https://doi.org/10.1007/s12206-012-0212-2.

Shan, D., Chai, Y.H., Zhou, X. and Khan, I. (2019), "Tension identification of suspenders with supplemental dampers for through and half-through arch bridges under construction", *J. Struct. Eng.*, **145**(3), 1-11. https://doi.org/10.1061/(ASCE)ST.1943-541X.0002255.

Wang, D.H. and Liao, W.H. (2011), "Magnetorheological fluid dampers: A review of parameteric modelling", *Smart Mater. Struct.*, **20**(2). https://doi.org/10.1088/0964-1726/20/2/023001.

Wu, B., Shi, P., Wang, Q., Guan, X. and Ou, J. (2010), "Performance of an offshore platform with MR dampers subjected to ice and earthquake", *Struct. Control Health Monit*., **18**(6), 682-697. https://doi.org/10.1002/stc.398.

Yang, C.K. and Kim, M.H. (2009), "Linear and nonlinear approach of hydropneumatic tensioner modeling for spar global performance", *J. Offshore Mech. Arcti*., **132**(1), 21.

Yang, M.G., Li, C.Y. and Chen, Z.Q. (2013), "A new simple non-linear hysteretic model for MR damper and verification of seismic response reduction experiment", *Eng. Struct*., **52**, 434-445. https://doi.org/10.1016/j.engstruct.2013.03.006.

Yang, M.G., Li, C.Y. and Chen, Z.Q. (2013), "A new simple non-linear hysteretic model for MR damper and verification of seismic response reduction experiment", *Eng. Struct.*, **52**, 434-445. https://doi.org/10.1016/j.engstruct.2013.03.006.

Zainuddin, Z., Kim, M.H., Kang, H.Y. and Bhat, S. (2018), "Incorporating magneto-rheological damper into riser tensioner system to restrict riser stroke in moderate-size semisubmersibles", *Proceedings of the Offshore Technology Conference*, Houston.